Gas-Phase Kinetics of Neutral Transition Metal Atoms: Reactions of Y through Mo with Alkanes and Alkenes at 300 K

John J. Carroll, Kerstin L. Haug, and James C. Weisshaar*

Contribution from the Department of Chemistry, University of Wisconsin–Madison, Madison, Wisconsin 53706

Received January 14, 1993

Abstract: We survey the reactivity of ground-state, neutral transition metal atoms from the left-hand side of the 4d series (Y through Mo) with eight alkanes and alkenes. Effective bimolecular rate constants are measured in 0.5–0.8 Torr of He in a fast flow reactor at 300 K with laser-induced fluorescence detection. None of the four ground-state metal atoms reacts with linear alkanes. Mo reacts slowly and Y, Zr, and Nb react rapidly with alkenes. From the absence of a measureable pressure dependence of the rate constant over the limited He range of 0.5–0.8 Torr, we infer that bimolecular elimination chemistry occurs. We relate the pattern of reactivity to recent *ab initio* calculations of the geometry and binding energy of $M–C_2H_4$ and $H–M–C_2H_3$ for 4d-series transition metals.

I. Introduction

Ligated transition metals are catalysts in a wide variety of solution-phase reactions. The Ziegler–Natta process for polymerization of ethylene is one important example.[1] In the gas phase, the study of bare transition metal atom reactivity provides a particularly simple view of fundamental metal–hydrocarbon interactions, unencumbered by complications due to solvent and ligands. These same relatively simple gas-phase reactions are becoming amenable to study by *ab initio* quantum chemistry. Quantitative comparison of theory and experiment can calibrate *ab initio* techniques and provide new insights into elementary reaction mechanisms.

While reactions of bare gas-phase metal *cations* with hydrocarbons have been studied in great detail,[2] neutral metal atom chemistry has been less extensively explored. The neutral atoms may well provide better models of solution-phase metal centers than the metal cations for several related reasons. Like typical solution-phase reactions, neutral M + hydrocarbon reactions in the gas phase often involve substantial potential energy barriers. We are beginning to understand the electronic nature of these barriers. In contrast, the long-range, ion-induced dipole interaction renders bare M^+ + hydrocarbon potentials anomalously attractive compared with condensed-phase systems. In addition, the nature of the bonding between neutral M and C_2H_4 for example, is more closely related to the bonding between ligated metals and C_2H_4 in the solution phase. Recent *ab initio* calculations[3] indicate that the $M^+–C_2H_4$ interaction is primarily electrostatic rather than covalent. In contrast, neutral metal atoms bind covalently with C_2H_4, displaying a rich variety of bonding schemes involving different electron spins and metal atom orbital occupancies.[4]

Our group and others have recently reported on the chemical kinetics of neutral 3d-series metal atom reactions with small alkanes and alkenes.[5,6] None of the 3d-series neutrals reacts with linear alkanes, while Sc, Ti, V, and Ni react with alkenes. The absence of pressure dependence strongly suggests that bimolecular elimination reactions occur, but we have determined neither the mass nor the structure of the products. Promotion energies from $3d^{x-2}4s^2$ ground states to low-spin, $3d^{x-1}4s^1$ excited states more suitable for bonding help to explain which metal atoms react with alkenes and which do not. Most recently, we found that the Pd ground state ($4d^{10}$) reacts highly efficiently with alkenes and moderately efficiently with C_2H_6 and larger linear alkanes.[7] All of the Pd reactions have a substantial termolecular component. *Ab initio* calculations[8] indicate that the collisionally stabilized Pd(alkane) products are long-range, η^2 complexes.

In this paper we extend our survey of chemical kinetics to the neutral metal atoms from the left-hand side of the 4d series: Y, Zr, Nb, and Mo. Neither Y, Zr, Nb, nor Mo react with linear alkanes at 300 K. For M + alkene reactions, the effective bimolecular rate constant at 300 K in 0.5–0.8 Torr of He helium buffer gas is 10 to 30 times greater for each 4d-series metal than for its 3d-series congener. For the M + alkene reactions, the rate constant increases with alkyl chain length. The rate constants for a given alkene follow the pattern $k_{Nb} > k_{Zr} \geq k_Y \gg k_{Mo}$. The absence of pressure dependence suggests that a bimolecular elimination mechanism contributes substantially to the metal–alkene chemistry.

Increasingly powerful *ab initio* electronic structure techniques have recently been applied to the problems of transition metal atom association with ethylene[4,9] and insertion into the C–H bond of CH_4 and the C–C bond of C_2H_6.[10,11] The recent systematic studies of $M–C_2H_4$ and $H–M–C_2H_3$ bonding for the entire 4d series[4] are particularly helpful in understanding our kinetics

(1) For an overview of solution-phase reactions that break C–H and C–C bonds, see: *Perspectives in the Selective Activation of C–H and C–C Bonds in Saturated Hydrocarbons*; Meunier, B., Chaudret, B., Eds.; Scientific Affairs Division-NATO: Brussels, 1988. For an overview of Ziegler–Natta chemistry, see: Pasquon, I.; Giannini, U. in *Catalysis, Science, and Technology*; Anderson, J. R., Boudart, M., Eds.; Springer-Verlag: Heidelberg, 1984; Vol. 6, pp 65–159.

(2) For a comprehensive review of M^+ chemistry, see: Eller, K.; Schwarz, H. *Chem. Rev.* **1991**, *91*, 1121.

(3) Sodupe, M.; Bauschlicher, C. W., Jr.; Langhoff, S. R.; Partridge, H. *J. Phys. Chem.* **1992**, *96*, 2118.

(4) (a) Blomberg, M. R. A.; Siegbahn, P. E. M.; Svensson, M. *J. Phys. Chem.* **1992**, *96*, 9794. (b) Siegbahn, P. E. M.; Blomberg, M. R. A.; Svensson, M. *J. Am. Chem. Soc.*, in press.

(5) (a) Ritter, D.; Weisshaar, J. C. *J. Am. Chem. Soc.* **1990**, *112*, 6425. (b) Ritter, D.; Carroll, J. J.; Weisshaar, J. C. *J. Phys. Chem.* **1992**, *96*, 10636. (c) Ritter, D. Ph.D. Thesis, Department of Chemistry, University of Wisconsin–Madison, 1990.

(6) (a) Mitchell, S. A. In *Gas Phase Metal Reactions*; Fontijn, A., Ed.; Elsevier: Amsterdam, 1992. (b) Parnis, J. M.; Mitchell, S. A.; Hackett, P. *J. Phys. Chem.* **1990**, *94*, 8152. (c) Mitchell, S. A.; Hackett, P. *J. Chem. Phys.* **1990**, *93*, 7822. (d) Brown, C. E.; Mitchell, S. A.; Hackett, P. *Chem. Phys. Lett.* **1992**, *191*, 175. (e) Blitz, M. A.; Mitchell, S. A.; Hackett, P. *J. Phys. Chem.* **1991**, *95*, 8719.

(7) Carroll, J. J.; Weisshaar, J. C. *J. Am. Chem. Soc.*, in press.

(8) Blomberg, M. R. A.; Siegbahn, P. E. M.; Svenson, M. *J. Am. Chem. Soc.* **1992**, *114*, 6095.

(9) Widmark, P. O.; Roos, B. O.; Siegbahn, P. E. M. *J. Phys. Chem.* **1985**, *89*, 2180.

0002-7863/93/1515-6962$04.00/0

results. We examine the observed pattern of reactivity with alkenes in the framework of simple donor–acceptor models of M–alkene bonding,[12] including electron promotion and sd-hybridization to relieve repulsive interactions at long range.[13] We suggest that variations in orbital sizes, electron configuration, spin multiplicity, and promotion energy combine to determine the height of the adiabatic potential energy barrier to formation of long-lived M(alkene) complexes, which in turn limits the 300 K rate constant.

II. Experimental Section

The kinetics technique uses a sputtering source to produce gas-phase transition metal atoms (M) in a fast flow of He buffer gas. Laser induced fluorescence (LIF) monitors the decay of the metal atom concentration vs hydrocarbon number density. The flow reactor has been used for transition metal ion kinetics studies[14] and more recently for neutral metal atom studies.[5,15] In the present work, the reaction length from the hydrocarbon gas inlet to the detection region is 74 cm. The average bulk flow speed is 6240 ± 160 cm/s in the reaction region. A thermistor indicates that the temperature in the reaction zone 74 cm downstream of the source is 300 ± 5 K.

The hydrocarbon gas is added midstream through showerhead inlets oriented upstream relative to the He flow. Flow of hydrocarbon is regulated by a needle valve or a flow controller and monitored by a mass flow meter (Tylan). The hydrocarbon gases, ethene (Matheson, >99.5%), propene (Matheson or Liquid Carbonic, >99.0%), 1-butene (Matheson, >99.0%), *trans*-2-butene (Matheson, >95%), *cis*-2-butene (Matheson, >95%), isobutene (Matheson or Agfa, >99.0%), ethane (Matheson, >99.95%), propane (Matheson, >99.0%), *n*-butane (Matheson, >99.0%), and cyclopropane (Matheson, >99.0%), are used directly from the bottle. Because flow meter response is not linear with gas flow, we have calibrated the flow meters with each reactant gas.

Metal atom reactant number density is monitored by unsaturated LIF with either a homemade pulsed dye laser pumped by an excimer laser (Lumonics EX-520, XeCl, 10 Hz, 10 ns fwhm) or a commercially manufactured dye laser (Lumonics HD-300) pumped by the third harmonic output of a Nd:YAG laser (Lumonics HY-600, 10 Hz, 10 ns fwhm). To avoid saturation, the dye laser beam is filtered to admit only 10–100 μJ/pulse into the detection region. The low-lying electronic terms of each metal atom are listed in Table I. Metal atoms are detected with spin–orbit level resolution. Table II summarizes the atomic transitions used to study each metal atom. A wavelength scan checks the purity of the spectrum; lines are then selected for kinetics studies. We observe clean, sharp lines. Saturated LIF spectra indicate that the populations of spin–orbit levels within the ground term are roughly Boltzmann at 300 K. All of the intense lines in the spectra are due to transitions from the ground term.

The simplest kinetics mechanism consistent with the data is a single reaction step:

$$\mathrm{M} + \text{alkene} \xrightarrow{k_1} \text{product 1} \qquad (1)$$

where k_1 could include both bimolecular and termolecular components. Other more complicated kientics models are discussed elsewhere.[5b,c] By measuring the logarithmic attenuation of metal atom number density (M) vs hydrocarbon number density (hc) at fixed mean reaction time $t_{rxn} = z_{rxn}/v_M$, we obtain the *effective bimolecular rate constant* k_1 from the pseudo-first-order expression $\ln[(M)/(M)_0] = -k_1(hc)t_{rxn}$. The ratio $(M)/(M)_0$ is measured as the ratio of time-integrated metal atom fluorescence signal with and without hydrocarbon reactant flow; z_{rxn} is the length of the reaction zone; and v_M is the mean axial speed of the metal atoms, which is larger than the bulk flow velocity due to loss of metal atoms at the walls. At 0.8 Torr of He, $v_M = 9070 \pm 250$ cm s^{-1}, as determined earlier.[5b,c]

Figure 1 shows examples of the logarithmic plots. Linear least-squares fitting produces the effective bimolecular rate constant k_1, which could include both bimolecular and termolecular components.

Collisional cascade of electronically excited states in the reaction zone has negligible effect on the ground-state rate constants. Quenching to the ground state on a time scale similar to that of the ground-state reaction would lead to nonlinear semilog plots, which are not observed. Within the ground term we observe no discernible effect of initial spin–orbit level on the reaction rate constant. Either all the spin–orbit levels probed react at the same rate, or collisional interconversion of spin–orbit levels is fast compared with chemical reaction in our experimental conditions.

Table I. Low-Lying Electronic Term Energies (10^3 cm^{-1}) of Selected 3d- and 4d-Series Transition Metal Atoms[a]

	configuration and term							
atom	$d^{x-2}s^2$		$d^{x-1}s$		$d^{x-2}sp$		d^x	
	^2D		^4F	^2F	^4F	^2D	^4F	^2D
Sc	0.0		11.5	14.9	15.8	16.0	33.7	36.2
Y	0.0		11.0	15.3	15.4	15.8	29.3	
	^3F	^1D	^5F	^3F	^5G	^3F	^5D	^3P
Ti	0.0	7.0	6.5	11.5	16.0	19.2	28.7	34.2
Zr	0.0	4.4	4.7	11.3	15.3	16.3	21.4	
	^4F	^2G	^6D	^4D	^6G	^4D	^6S	^4D
V	0.0	10.7	2.0	8.3	16.5	20.5	19.9	34.0
Nb	1.5	8.5	0.0	8.5	17.4	20.3	10.7	
	^5D	^3P	^7S	^5S	^7F	^5P	^5D	^3H
Cr	8.1	23.8	0.0	7.6	25.4	29.7	35.5	
Mo	11.8	22.4	0.0	10.8	29.5	33.5	25.7	34.9
	^3F	^1D	^3D	^1D	^5D	^3G	^1S	
Ni	0.2	12.8	0.0	2.7	26.0	30.4	14.0	
Pd	27.2		7.7	11.7	50.9		0.0	

[a] Energies in 10^3 cm^{-1}. Entries are the average of spin–orbit level energies within each term weighted by the degeneracy $(2J + 1)$. The lowest average energy is defined as zero. For each configuration, the lowest energy terms of each important spin multiplicity are included when available. Data from ref 16.

Table II. Laser-Induced Fluorescence Transitions[a]

atom	transition	energy (cm^{-1})
Y	$^2D_{3/2} \leftarrow {}^2D_{3/2}$	24 131
Y	$^2F_{5/2} \leftarrow {}^2D_{5/2}$	23 988
Zr	$^3G_3 \leftarrow {}^3F_2$	25 730
Zr	$^3F_3 \leftarrow {}^3F_3$	25 873
Nb	$^6F_{1/2} \leftarrow {}^6D_{1/2}$	23 985
Nb	$^6F_{3/2} \leftarrow {}^6D_{3/2}$	24 011
Mo	$^7P_3 \leftarrow {}^7S_3$	25 872

[a] Assignments from ref 16.

III. Results

A. Rate Constants in 0.5 and 0.8 Torr of He. We have studied the reactions of four neutral transition metal atom ground states with ten hydrocarbons at 0.80 ± 0.05 Torr of He and 300 ± 5 K. The ground states probed (Table II) are Y($^2D_{3/2}$,d^1s^2), Zr($^3F_2$,d^2s^2), Nb($^6D_{1/2}$,d^4s^1), and Mo($^7S_3$,d^5s^1). An atomic state[16] is labeled by its electron configuration, total electron spin (S), orbital angular momentum (L), and total angular momentum (J), as embodied in the symbol $^{2S+1}L_J$. We use Russell–Saunders coupling in spite of the substantial spin–orbit coupling in the 4d series because the spin–orbit levels associated with each atomic term typically do not interleave those associated with other terms.

The effective bimolecular rate constants in 0.5 and 0.8 Torr of He are collected in Table III. Each reported rate constant at 0.8 Torr is the mean of two to four individual determinations. The sensitivity limit of the apparatus is $k_1 \geq 3 \times 10^{-14}$ cm^3 s^{-1}. The error estimates in Table III refer to the *precision* of the 0.8

(10) (a) Blomberg, M. R. A.; Siegbahn, P. E. M.; Nagashima, U.; Wennerberg, J. *J. Am. Chem. Soc.* **1991**, *113*, 424. (b) Blomberg, M. R. A.; Siegbahn, P. E. M.; Svensson, M. *J. Phys. Chem.* **1991**, *95*, 4313. (c) Svensson, M.; Blomberg, M. R. A.; Siegbahn, P. E. M. *J. Am. Chem. Soc.* **1991**, *113*, 7076.

(11) (a) Low, J. J.; Goddard, W. A., III *J. Am. Chem. Soc.* **1984**, *106*, 8321. (b) Low, J. J.; Goddard, W. A., III *Organometallics* **1986**, *5*, 609.

(12) Dewar, M. J. S. *Bull. Soc. Chim. Fr.* **1951**, *18*, C71. Chatt, J.; Duncanson, L. A. *J. Chem. Soc.* **1953**, 2939.

(13) Langhoff, S. R.; Bauschlicher, C. W., Jr. *Annu. Rev. Phys. Chem.* **1988**, *39*, 181.

(14) Tonkyn, R.; Weisshaar, J. C. *J. Phys. Chem.* **1986**, *90*, 2305. Tonkyn, R.; Ronan, M.; Weisshaar, J. C. *J. Phys. Chem.* **1988**, *92*, 92. Tonkyn, R.; Weisshaar, J. C. *J. Am. Chem. Soc.* **1986**, *108*, 7128.

(15) Ritter, D.; Weisshaar, J. C. *J. Phys. Chem.* **1990**, *94*, 4907.

(16) Moore, C. E. *NBS Circ. No. 467*; U.S. Dept. of Commerce, Washington, DC, 1949; Vols. I–III.

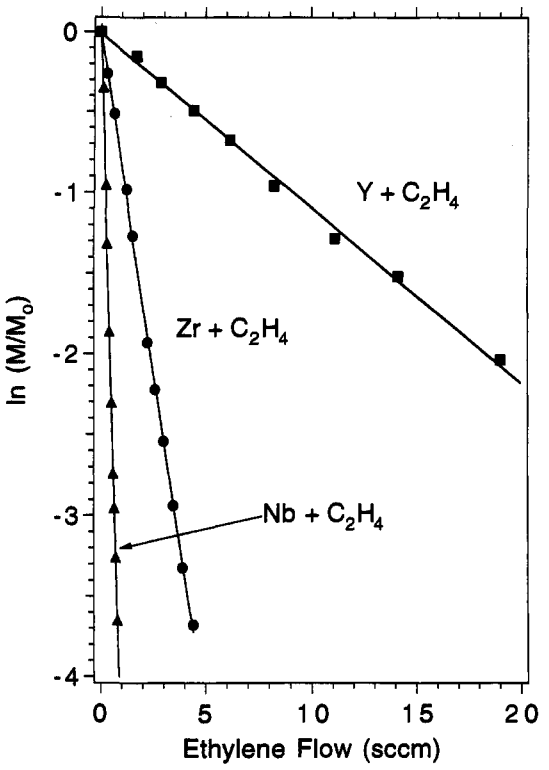

Figure 1. Semilogarithmic plots of metal atom density vs hydrocarbon flow for the M + C_2H_4 reactions indicated at 300 K and 0.8 Torr of He.

Torr rate constants. They represent the larger of ±10%, the range of two values, or ±1 standard deviation of the mean of multiple measurements. The *absolute accuracy* of the observed rate constants is estimated as ±30%, limited by the uncertainties in t_{rxn} and gas flow calibrations, incomplete reagent mixing, source instability, and random noise in the data.

We observe no reaction for any of the metals on the left-hand side of the 4d series with the linear alkanes ethane, propane, and *n*-butane. Cyclopropane reacts slowly with Y, Zr, and Nb. Y, Zr, and Nb atoms react rapidly with all of the alkenes studied. Mo reacts with alkenes larger than C_2H_4, albeit very slowly. All four metals show an increase in reaction rate as the number of carbon atoms in the alkene increases. For each alkene, reaction rates decrease in the following order: $k_{Nb} > k_{Zr} > k_Y \gg k_{Mo}$.

We also measured total removal rates of the first excited spin–orbit level of Y ($^2D_{5/2}$, 530 cm^{-1} excitation energy), Zr ($^3F_3$, 570 cm^{-1}), and Nb ($^6D_{3/2}$, 154 cm^{-1}) by collisions with selected alkenes. The LIF transitions are included in Table II. Measured rate constants are always the same within experimental uncertainty for the lowest two spin–orbit levels. This indicates either that both levels react at the same rate or that collisional interconversion of the two spin–orbit levels within the ground term is rapid compared with chemical reaction. In the latter case, we would measure a Boltzmann average of level-specific rate constants. If spin–orbit excitation energy were useful in surmounting potential energy barriers and collisional interconversion of spin–orbit levels were slow, then at least the Y and Zr excited levels might have been expected to react more rapidly than the ground states.

In an attempt to determine whether third-body stabilization contributes significantly to the observed rate constants, we carried out measurements at the lower He pressure of 0.5 Torr. The hollow cathode discharge is less stable at the lower pressure and cannot be used below 0.5 Torr in the main flow tube. Rate constants measured at 0.5 Torr are listed in Table III. Each entry represents one or two determinations of k_1 from ten to fifteen data points of metal atom LIF signal vs flow of hydrocarbon. Comparison with the 0.8 Torr rate constants shows no systematic change in rate constant with pressure within the estimated relative uncertainty of ±20%. For the 14 reactions for which we have measured rate constants at both 0.5 and 0.8 Torr, the two results agree within 10% in 12 cases and within 20% in all 14 cases.

If a termolecular reaction were in the linear, low-pressure regime of effective bimolecular rate constant vs He pressure, the measured rate constant k_1 would increase by a factor of 1.6 as the He pressure increased from 0.5 to 0.8 Torr. We can estimate a lower limit on the fraction of the measured k_1 due to bimolecular, as opposed to termolecular, reaction at 0.8 Torr of He by writing the ratio $R = k_1(0.8\ \text{Torr})/k_1(0.5\ \text{Torr}) = [k_{bi} + k_{ter}(0.8\ \text{Torr})]/[k_{bi} + k_{ter}(0.5\ \text{Torr})]$. Here k_{bi} is the bimolecular component and k_{ter}(He) is the termolecular component of the measured k_1. The experimental estimate $R \leq 1.4$, which allows a generous 40% uncertainty in the ratio of measured rate constants at 0.8 and 0.5 Torr, implies that *at least one-quarter* of the measured k_1 is due to the bimolecular component k_{bi}. It is much more likely that $R \leq 1.2$, which implies that *at least one-half* of k_1 is due to k_{bi}. The data are consistent with the possibility that k_1 is dominated by bimolecular chemistry at 0.8 Torr of He.

B. Limits on Activation Energies from 300 K Reaction Efficiencies. Since we study reactions from a Boltzmann distribution of translational energies at 300 K and a specific electronic state of M, the reactant energy distribution is well-defined. We can use estimated reaction efficiencies to set limits on the activation energies of each observed reaction. For those reactions that occur in the flow tube at 300 K, we first estimate the hard-sphere collision rate constant k_{hs} from approximate atomic and molecular sizes[17] and calculate the average number of hard-sphere collisions required for chemical reaction. Typical values of k_{hs} are in the range 2×10^{-10} to 4×10^{-10} $cm^3\ s^{-1}$. The observed rate constants range from 0.7×10^{-12} to 390×10^{-12} $cm^3\ s^{-1}$. The largest rate constants match estimated values of k_{hs} within their uncertainty. The lower limit of 3×10^{-14} $cm^3\ s^{-1}$ on the measured rate constants means we cannot observe reactions that require more than about 10^4 hard-sphere collisions to occur.

Since k_BT is only 200 cm^{-1} = 0.6 kcal mol^{-1} at 300 K, only those reactions with rather small activation energies in a narrow range will be observed in our flow tube. Assuming the Arrhenius dependence

$$k_1(T) = A \exp(-E/k_BT) \qquad (2)$$

and using the estimated hard-sphere collision rate constant k_{hs} as an upper bound on the pre-exponential factor A, we can convert k_1/k_{hs} into an upper bound E_{max} on the activation energy. For example, when $k_1/k_{hs} = 0.1$, the activation energy can be no larger than E_{max} = 1.4 kcal mol^{-1}; when $k_1/k_{hs} = 0.01$, E_{max} = 2.8 kcal mol^{-1}; and when $k_1/k_{hs} = 0.001$, E_{max} = 4.2 kcal mol^{-1}. Since we have not measured $k(T)$, the true activation energy might be substantially smaller than the calculated E_{max}. It could be zero if the pre-exponential factor is much smaller than k_{hs}, i.e., if there is a steric requirement for reaction to occur. For those reactions not observed ($k < 10^{-14}$ $cm^3\ s^{-1}$), either the activation energy is >5 kcal mol^{-1} or the pre-exponential factor is quite small.

IV. Discussion

A. Overview of Previous Results. Interactions of hydrocarbons with neutral 4d-series metal atoms have not been explored extensively. Studies in cryogenic matrices have concentrated on atoms from the right-hand side of the 4d series such as Pd and Ag.[18] In the gas phase, several studies have explored 4d-series neutral metal atom and cluster reactivity using photoionization

(17) Atomic diameters taken as 2 $\langle r \rangle$ for the $(n + 1)$s orbital from ref 26. Molecular diameters estimated from: Hirschfelder, J. O.; Curtis, C. F.; Bird, R. B. *Molecular Theory of Gases and Liquids*; Wiley: New York, 1954; Table IA.

(18) See, for example: (a) Hisatsune, I. C. *J. Catalysts* **1982**, *74*, 9. (b) Andrews, M. P.; Ozin, G. A. *J. Phys. Chem.* **1986**, *90*, 2922.

Table III. Effective Bimolecular Rate Constants, k_1 (10^{-12} cm^3 s^{-1}), for Reactions of Transition Metal Atoms with Hydrocarbons at 0.80 ± 0.05 and 0.50 ± 0.05 Torr of He and 300 ± 5 K[a]

	Y($^2D_{3/2}$)		Zr($^3F_2$)		Nb($^6D_{1/2}$)		Mo($^7S_3$)	
reactant	0.8 Torr	0.5 Torr	0.8 Torr	0.5 Torr	0.8 Torr	0.5 Torr	0.8 torr	0.5 torr
ethene	8.2 ± 0.8	7.7 ± 1.6	59 ± 6	59 ± 12	314 ± 31	324 ± 65	NR	NR
propene	141 ± 14	138 ± 28	153 ± 15	149 ± 30	360 ± 36	333 ± 67	0.38 ± 0.19	–
1-butene	143 ± 14	144 ± 29	156 ± 16	150 ± 30	390 ± 39	375 ± 75	2.08 ± 0.41	2.30 ± 0.46
trans-2-butene	–	–	150 ± 15	–	–	–	–	–
cis-2-butene	–	–	187 ± 19	–	–	–	–	–
isobutene	234 ± 23	213 ± 43	216 ± 22	223 ± 45	384 ± 38	–	1.03 ± 0.10	–
cyclopropane	0.70 ± 0.07	0.61 ± 0.12	0.66 ± 0.13	0.64 ± 0.13	3.04 ± 0.30	–	NR	–
ethane	NR	NR	NR	NR	–	–	NR	–
propane	NR	NR	NR	–	NR	–	NR	–
n-butane	NR	NR	NR	–	NR	–	NR	–

[a] NR means no reaction observed, i.e., $k_1 < 3 \times 10^{-14}$ cm^3 s^{-1}; dash means no information on this reaction. At 0.8 Torr uncertainties refer to the *precision* of the measurements; they are the larger of ±10%, the range of two values, or ±1 standard deviation of the mean of three values. At 0.5 Torr uncertainties are 20%, our estimate of the *precision*. Absolute accuracies are estimated as ±30%.

Table IV. Comparison of Reactivity of 3d- and 4d-Series Congeners with Hydrocarbons in 0.80 Torr of He at 300 ± 5 K[a] (Effective Bimolecular Rate Constants in 10^{-12} cm^3 s^{-1})

atom	ethene	propylene	1-butene	*n*-butane
Sc	NR	9.5 ± 1	14 ± 1	NR
Y	8.2 ± 0.8	141 ± 14	143 ± 14	NR
Ti	NR	6.2 ± 0.6	7.1 ± 0.7	NR
Zr	59 ± 6	153 ± 15	156 ± 16	NR
Y	NR	9.6 ± 1	14 ± 1	NR
Nb	314 ± 31	360 ± 36	390 ± 39	NR
Cr	NR	NR	NR	NR
Mo	NR	0.38 ± 0.19	2.08 ± 0.41	NR
Ni	0.5 ± 0.05	11 ± 4	140 ± 30	NR
Pd	15.8 ± 1.6	189 ± 19	378 ± 38	4.6 ± 0.5

[a] NR means no reaction observed, i.e., $k_1 < 3 \times 10^{-14}$ cm^3 s^{-1}. Uncertainties are the larger of ±10% or ±2 standard deviations of the mean. Absolute accuracies are ±30%. 3d-series data are from ref 5b. Pd data are from ref 7.

mass spectrometry to identify products. El-Sayed and coworkers,[19] as well as Kaldor and co-workers[20] have studied Nb cluster reactions extensively. Both groups detected H_2 elimination products for reaction of Nb_x with alkenes. No reaction was observed between cyclohexane and Nb atom or Nb_x clusters. Cox, Kaldor, and co-workers have examined the reactivity of methane with a variety of metal atoms and clusters. Within the 4d series they found methane to be inert towards Nb atoms,[20] Rh atoms,[21] and Pd atoms.[22]

B. Electronic Effects on Metal Atom Reactivity. Our results can be summarized as follows. The ground states of neither Y, Zr, Nb, nor Mo react with linear alkanes at 300 K (Table III). Y, Zr, and Nb react slowly with cyclopropane and very rapidly with alkenes. Mo reacts only with alkenes, and those reactions are quite slow. In all observed cases, the absence of a pressure dependence in the rate constants measured at 0.5 and 0.8 Torr suggests a bimolecular reaction mechanism, i.e., elimination of H_2 or alkane. Each of the 4d-series metals Y, Zr, Nb, Mo, and Pd reacts with alkenes at least 10 times faster than its 3d-series congener Sc, Ti, V, Cr, and Ni, respectively (Table IV). We seek explanations for our observations based on simple models of M–hydrocarbon binding, variations in the electronic structure of the bare metal atom, and recent *ab initio* calculations of the structure of M–C_2H_4 complexes.[4]

1. Overview of Metal Atom Structure. The size and energy of atomic orbitals influence the strength of metal–ligand chemical bonding.[10] In addition, since the ground state of the metal atom is almost always ill-suited for bonding due to its electron configuration or spin multiplicity or both, atomic promotion energies should strongly influence ground-state reactivity by determining the energetics of key potential surface intersections.[23,24]

The low-lying electronic states of the 3d- and 4d-series neutral metal atoms are well-known (Figure 2 and Table I).[8] The order of low-lying states results from a competition between electron configuration stability (orbital energies) and electron exchange effects that favor high-spin states.[10] The effective nuclear charge felt by both d and s electrons increases from left to right across a transition series, but the *n*d orbital energy stabilizes more rapidly than (*n*+1)s. This lowers the energy of d^x configurations relative to $d^{x-1}s^1$ and of $d^{x-1}s^1$ configurations relative to $d^{x-2}s^2$ as nuclear charge increases. At the same time, electron exchange interactions stabilize high-spin terms relative to low-spin terms. Formation of covalent chemical bonds involves a loss of favorable exchange interactions from high-spin ground states, a well understood effect that is most severe in the middle of each transition series.[25]

In the 3d series, most of the ground states (Sc, Ti, V, Mn, Fe, Co, and Ni) have $3d^{x-2}4s^2$ configurations; the lowest excited states are high-spin $3d^{x-1}4s^1$. In Cr and Cu, the $3d^54s^1$ and $3d^{10}4s^1$ configurations are the ground states. In the 4d series high-spin $4d^{x-1}5s^1$ ground states are common. Only for Y, Zr, and Tc does the $4d^{x-2}5s^2$ configuration lie lowest in energy. Palladium ($4d^{10}$) is unique among the transition metals in having a d^xs^0 ground-state configuration. In addition, the ratio $\langle r\rangle_{(n+1)s}/\langle r\rangle_{nd}$ is smaller in the 4d series than in the 3d series, i.e., the 4d orbital is larger compared with 5s than is 3d compared with 4s (Table V).[26] Finally, spin–orbit interaction is substantially stronger in the 4d series, which can affect the height of adiabatic potential energy barriers as described below.

2. Metal–Alkene Bonding Mechanisms. The electronic requirements for metal atom insertion into a C–H bond of an alkane or alkene, for formation of a M–alkene donor–acceptor complex, and for formation of a metallacyclopropane ring from M + alkene are all quite similar, as described by Hoffmann and co-workers[27] and most recently by Blomberg *et al.*[4] Since the M + alkene reactions are by far the most efficient, we focus the discussion on simple models of M–alkene bonding. The absence of pressure dependence for most of the rate constants leads us to strongly suspect that much of the observed chemistry is in fact bimolecular, H_2 elimination chemistry. In using models of M–alkene bonding to explain differences is observed reaction rates, we are assuming

(19) (a) St. Pierre, R. J.; El-Sayed, M. A. *J. Phys. Chem.* **1987**, *91*, 763. (b) St. Pierre, R. J.; Chronister, E. L.; Song, L.; El-Sayed, M. A. *J. Phys. Chem.* **1987**, *91*, 4648. (c) Song, L.; El-Sayed, M. A. *J. Phys. Chem.* **1990**, *94*, 7907.
(20) Zakin, M. R.; Cox, D. M.; Kaldor, A. *J. Phys. Chem.* **1987**, *91*, 5224.
(21) Zakin, M. R.; Cox, D. M.; Kaldor, A. *J. Chem. Phys.* **1988**, *89*, 1201.
(22) Fayet, P.; Kaldor, A.; Cox, D. M. *J. Chem. Phys.* **1990**, *92*, 254.
(23) Weisshaar, J. C. In *State-Selected and State-to-State Ion–Molecule Reaction Dynamics, Part I*; Ng, C.-Y., Ed.; Wiley: New York, 1992.
(24) Weisshaar, J. C. In *Gas Phase Metal Reactions*; Fontijn, A., Ed.; Elsevier: Amsterdam, 1992.
(25) Carter, E. A.; Goddard, W. A., III *J. Phys. Chem.* **1988**, *92*, 5679.
(26) Fischer, C. F. *The Hartree Fock Method for Atoms*; Wiley: New York, 1977.
(27) Saillard, J.-Y.; Hoffmann, R. *J. Am. Chem. Soc.* **1984**, *106*, 2006.

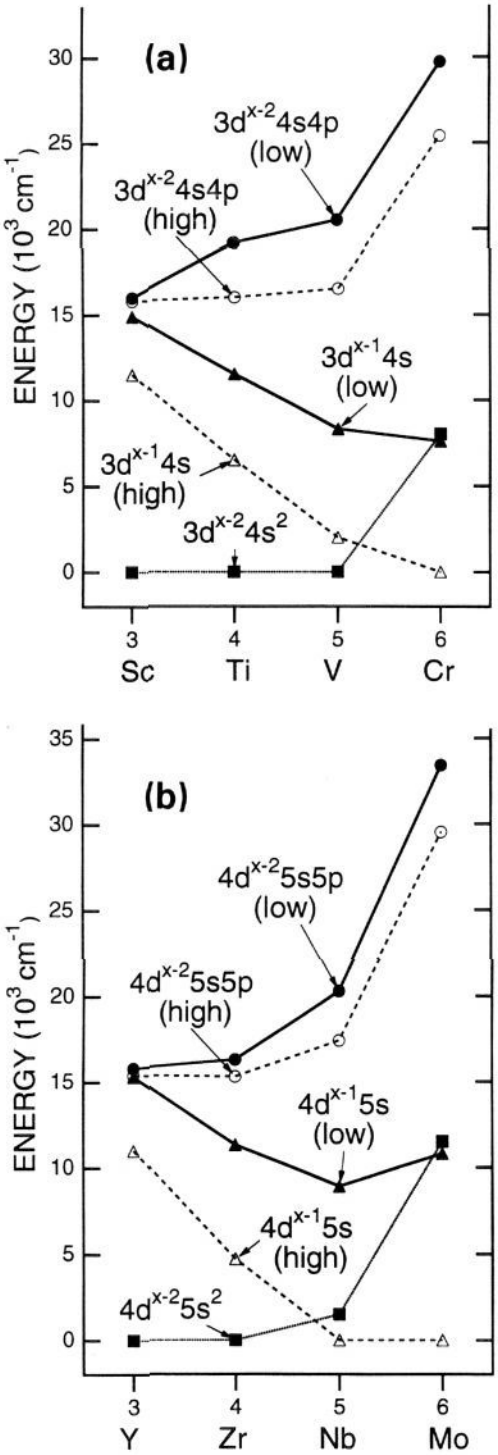

Figure 2. Low-lying electronic term energies of (a) 3d-series and (b) 4d-series neutral transition metal atoms. "High" and low" refer to spin multiplicities within each configuration. See Table I.

that the rate-limiting step in a possibly complicated, multistep mechanism is formation of a long-lived M–alkene complex. Even for H_2 elimination reactions that proceed by metal insertion into a C–H bond of alkene, initial formation of a long-lived M–alkene complex may be the rate-determining step. Furthermore, the same sd hybridization scheme that assists formation of a M–alkene complex also assists formation of H–M–C_2H_3,[4] so our arguments are relevant even if the reaction rate is limited by the barrier to C–H bond insertion.

The interaction between a transition metal atom and an alkene is often described in terms of the Dewar–Chatt–Duncanson

Table V. First Ionization Energy and Mean Orbital Radii (Å) for 3d- and 4d-Series Neutral Transition Metal Atoms[a]

atom	I_1 (eV)	$\langle r\rangle_{(n+1)s}$	$\langle r\rangle_{nd}$	$\langle r\rangle_{(n+1)s}/\langle r\rangle_{nd}$
Sc	6.54	2.09	0.89	2.4
Y	6.38	2.27	1.29	1.8
Ti	6.82	2.00	0.77	2.6
Zr	6.84	2.16	1.11	1.9
V	6.74	1.92	0.70	2.7
Nb	6.88	2.08	1.00	2.1
Cr	6.77	1.85	0.64	2.9
Mo	7.10	2.01	0.92	2.2
Ni	7.64	1.62	0.51	3.2
Pd	8.34	1.79	0.73	2.5

[a] Expectation values $\langle r\rangle$ are in Å for 3d and 4d and for 4d and 5s orbitals from Hartree–Fock calculations, ref 26. In all cases, orbitals come from the $d^{x-2}s^2$ configuration of lowest energy. I_1 data are from ref 16.

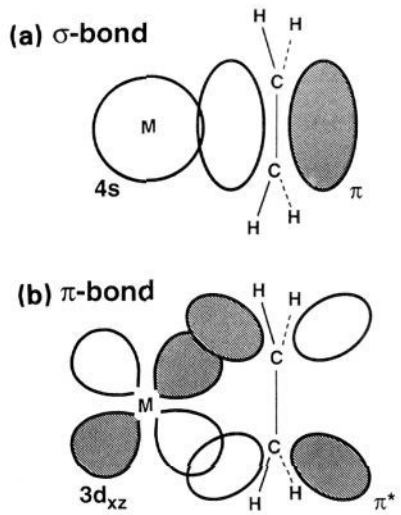

Figure 3. Schematic of the donor–acceptor model of M–alkene bonding: (a) alkene (π) → metal (4sσ, or a 4s–3d–3p hybrid σ orbital) donor–acceptor interaction; (b) metal (3dπ) → alkene (π^*) donor–acceptor interaction. The strong limit of these same interactions produces a metallacyclopropane structure with two M–C σ bonds.

(DCD) donor–acceptor model.[9] Bonding occurs via the simultaneous formation of two donor–acceptor bonds, as pictured schematically in Figure 3. The first bond involves donation of electrons from the alkene 2pπ orbital to a metal orbital of σ symmetry (a_1 in C_{2v} geometry). The metal acceptor orbital can be a linear combination of ndσ, $(n+1)$sσ, and $(n+1)$pσ. The simplest model invokes sd hybridization. The hybrid orbital $|sd_+\rangle = |s\sigma\rangle + |d\sigma\rangle$ is the acceptor orbital which concentrates probability density on the M–alkene approach axis. One or two s electrons on the metal evolve to occupy the lone pair orbital $|sd_-\rangle = |s\sigma\rangle - |d\sigma\rangle$, which relieves electron–electron repulsion by concentrating density near the plane perpendicular to the approach axis. The second bond involves "back-donation" from the singly or doubly occupied metal dπ orbital which lies in the M–C–C plane (b_2 symmetry in C_{2v} geometry) to the empty alkene 2pπ^* orbital, forming a π bond.

Formation of a metallacyclopropane is an extreme version of the same donor–acceptor model with shorter M–C and longer C–C bond lengths. The two doubly occupied molecular orbitals that represent the M–C bonds have the same a_1 and b_2 symmetries in C_{2v} geometry as the $|sd_+\rangle$ and $|d\pi\rangle$ orbitals of the donor–acceptor picture. In fact, the recent *ab initio* calculations of Blomberg *et al.*[4] find the low-spin metallacyclopropane structure the most stable M–C_2H_4 complex for M = Y, Zr, and Nb. The M–C bond is short, 2.07–2.15 Å, and the C–C bond is long, 1.51–1.54 Å, compared with 1.34 Å in bare C_2H_4. Estimated

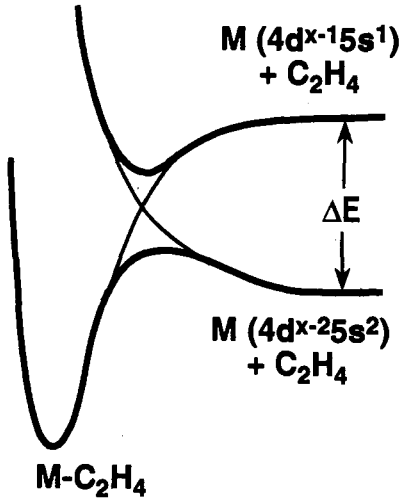

Figure 4. Schematic potential energy curves for reactions of Y and Zr with alkenes in C_{2v} approach geometries. The coordinate is the distance from the metal to the bisector of the C–C bond. The repulsive and attractive diabatic curves have the same spin, so the crossing is strongly avoided.

binding energies are 22–24 kcal mol^{-1} relative to ground state M + C_2H_4. The Mulliken populations show a +0.3 charge on the metal, indicating polarized M–C bonds. At slightly higher energy, the calculations also find donor–acceptor complexes with the 4sσ (a_1) and 4dπ (b_2) orbitals *singly occupied* for Y, Zr, and Nb. For Y, this $^2B_2$ complex matches the $^2A_1$ metallacyclopropane in electron spin. For Zr and Nb, the complex has high spin compared with the metallacyclopropane ($^5A_1$ vs $^3B_1$ for Zr, and $^6A_1$ vs $^4B_1$ for Nb). In the donor–acceptor complexes, the M–C bonds are longer (2.34–2.46 Å) and the C–C bond length is 1.41–1.42 Å, quite similar to bare C_2H_4.

While the calculations are very useful, they do not comment directly on the height of possible barriers between ground state M + alkene and the stable metallacyclopropane complexes (Y, Zr, Nb). For $d^{x-2}s^2$ ground states (Y, Zr), the potential between M and alkene is presumably repulsive at long range due to overlap of the large, doubly occupied $(n+1)$s orbital with the doubly occupied π orbital of the alkene.[5b] This explains the relative inertness of most 3d-series metal atoms, whose 4s orbital is much larger than 3d (Table V). In order to achieve close approach to an alkene, a $d^{x-2}s^2$ ground state atom must *hybridize* to relieve electron–electron repulsion and permit attractive alkene → metal donor–acceptor interactions. In the 3d series, we suggested that the promotion energies to the lowest $3d^{x-1}4s$ excited state M* of the proper spin to form sd hybrid orbitals can qualitatively explain why only Sc, Ti, V, and Ni react with alkenes at 300 K. While we focus on sd hybridization, the $(n+1)$p orbital of σ symmetry can also contribute by polarizing the metal acceptor orbital, especially on the left-hand side of each series. In the 4d series, Blomberg and co-workers find substantial Mulliken population in 5p for the metallacyclopropane ground states of Y, Zr, and Nb, whose promotion energies to $4d^{x-2}5s5p$ states are relatively small (Table I).

A large promotion energy, ΔE, to the appropriate excited state M* should correlate with a large potential barrier on adiabatic surfaces connecting ground-state M + alkene to the M–alkene complex, as shown schematically in Figure 4. For metal atoms with $d^{x-2}s^2$ ground states, including Y and Zr, the bound M–alkene complex correlates diabatically with an *excited state* asymptote M* + alkene with a low-spin, $d^{x-1}s^1$ configuration on the metal (Table I, Figure 2). Here diabatic means conserving orbital occupancy and electron spin multiplicity. For Y and Zr, the ground state matches the excited state in electron spin, so we expect the surface intersection to be strongly avoided. This apparently results in a small barrier on the *adiabatic* surface leading from ground state M + alkene to the M–alkene complex. For reaction of the same alkene with Y and Zr, the adiabatic barrier height should be roughly a constant fraction of the promotion energy ΔE. Accordingly, Zr reacts faster with C_2H_4 than Y. For Nb, a different model seems to apply, as discussed below.

Several additional factors contribute to the generally greater reactivity of the 4d-series atoms compared with their 3d-series congeners. The 4d orbital is larger than 3d, both in an absolute sense and relative to the size of the valence $(n+1)$s orbital (Table V). This has three effects. First, sd hybridization reduces electron–electron repulsion in the 4d series more effectively. Because the s and d orbitals are more similar in size, constructive and destructive interference in $|sd_+\rangle$ and $|sd_-\rangle$ is more pronounced at the distances most important for chemical bonding. Second, the larger absolute size of 4d orbitals permits stronger bonds to carbon and hydrogen. *Ab initio* studies have shown that 3d orbitals are two compact to overlap well with alkene orbitals.[13] The increased binding energy of M–alkene relative to M* + alkene for 4d-series metals helps to decrease adiabatic barrier heights (Figure 4). Third, the larger size of 4d relative to 5s means that chemical bonding interactions can begin earlier in the approach of M to alkene. This should attenuate long-range repulsions and further decrease barrier heights.

3. Trends in Reactivity. We begin our detailed comparison of the 3d and 4d series with the congener pairs Sc–Y and Ti–Zr. Y reacts with alkenes at least 10 times faster than Sc, and Zr reacts with alkenes at least 20 times faster than Ti. These differences in rate constant may well be due to rather subtle differences in adiabatic barrier height. If two reaction rate constants have the same pre-exponential factor (eq 2), then a factor of 20 difference in rate constants at 300 K requires a difference in activation energy of only $3k_BT$ = 600 cm^{-1} = 1.8 kcal mol^{-1}. All four atoms have $d^{x-2}s^2$ ground states and fairly low-lying $d^{x-1}s$ and $d^{x-2}sp$ excited states of both high and low spin. The pattern of low-lying state energies is remarkably similar for Sc and Y and for Ti and Zr (Table I). In particular, the promotion energy to the first low-spin $d^{x-1}s$ term is 400 cm^{-1} smaller for Sc than for Y (opposing the trend in rate constants) and only 200 cm^{-1} smaller for Zr than for Ti. We would expect differences in asymptotic energy to be attenuated in the difference of barrier heights, so the enhanced 4d-series reactivity does not arise from smaller promotion energies. Therefore we suggest that the enhanced reactivity of Y and Zr compared with Sc and Ti is primarily due to orbital size effects, as discussed above. The larger 4d orbital makes stronger bonds that begin to form at longer range.

So far Nb is the most reactive neutral transition metal atom with alkenes. Nb reacts with alkenes at least 30 times more rapidly than its 3d congener V (Table IV) and substantially more rapidly than Ni or Pd. Within the 4d series Nb is significantly more reactive than Y or Zr, while in the 3d series Sc, Ti, and V react quite similarly. The Nb + alkene effective bimolecular rate constant is essentially equal to the hard-sphere rate constant for the C_2H_4, C_3H_6, and 1-butene reactions. The absence of pressure dependence strongly suggests efficient bimolecular chemistry. By analogy to M^+ chemistry, the most likely bimolecular reaction is H_2 elimination.

There is apparently *no* adiabatic barrier to the close approach of the Nb ground state and alkene. This experimental fact is *not* easy to understand from promotion energies and the simple curve-crossing model of Figure 4. In comparing V and Nb, differences in both electron configuration and spin come into play. The Nb ground state is $4d^45s$ (^6D), while the V ground state is $3d^34s^2$ (^4F). Nb is more reactive than V in spite of the fact that its ground state has the wrong spin for formation of metallacyclopropane or insertion into a C–H bond. In this regard, the d^4s, ^6D ground state of Nb is comparable to the d^9 s, ^3D ground state

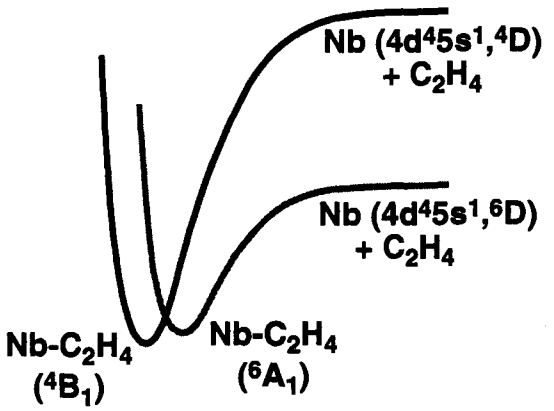

Figure 5. Schematic potential energy curves for reaction of Nb with alkenes. The $^6A_1$ well is a long-range, donor–acceptor complex, while the $^4B_1$ well is a metallacyclopropane. See ref 8.

of Ni, the most reactive 3d-series atom. In Nb, the promotion energy to d^4s, ^4D is 8500 cm^{-1}; in Ni, the promotion energy to d^9s, ^1D is only 2700 cm^{-1}. Yet Nb reacts with C_2H_4 on essentially every collision, while Ni reacts on 1 in 600 collisions.

Thus the model embodied in Figure 4 seems not to apply to Nb. Instead, we suggest that the $^6A_1$ donor–acceptor complex discovered in the recent *ab initio* work[4] provides a uniquely attractive initial binding mechanism for ground-state Nb + alkene collision partners, as pictured in Figure 5. The calculated binding energy of the sextet complex is a remarkable 24 kcal mol^{-1} relative to ground-state Nb + alkene, very similar to the energy of the $^4B_1$ metallacyclopropane. The Mulliken population of the $^6A_1$ complex is approximately $4d^45s^1$. This suggests that the complex is stabilized by *two half-bonds*, both donor–acceptor in nature: $4d\pi \rightarrow 2p\pi^*$ and $5s\sigma \leftarrow 2p\pi$. Hybridization to the metal configuration $(sd_-)^1d\pi^2d\delta^2$ is an alternative bonding scheme, but it would presumably give the population $4d^{4.5}5s^{0.5}$. The $^6A_1$ complex correlates with ground-state reactants in both spin and configuration. Moreover, the d^4s ground-state configuration of Nb should diminish long-range repulsive effects compared with d^3s^2, so there may well be no barrier between Nb(^6D) + C_2H_4 and the $^6A_1$ complex. If bimolecular bond-breaking chemistry indeed occurs, then the initially formed sextet Nb–alkene complex must eventually reach a quartet surface. The long lifetime of the $^6A_1$ complex provides sufficient *time* for this nominal change of spin to occur efficiently at short range, driven by the enhanced spin–orbit coupling in the 4d series.

Comparison of Cr and Mo suggests the importance of both enhanced spin–orbit interaction and stronger metal–ligand binding in the 4d series. For both atoms, the chemically inert d^5s, ^7S ground state lies substantially below the low-spin d^5s excited state appropriate for chemical bonding. In Cr the promotion energy to d^5s, ^5S is 7600 cm^{-1}, while in Mo the corresponding promotion energy is substantially *larger*, 10 800 cm^{-1}. Yet Cr is inert to alkenes, while Mo reacts, albeit quite slowly. The recent *ab initio* calculations[4] find a Mo–C_2H_4 ($^5B_2$) complex bound by only 6.5 kcal mol^{-1} relative to ground-state Mo + C_2H_4. The nature of the septet surface correlating with ground-state Mo + C_2H_4 is unclear. No septet well analogous to the sextet Nb–C_2H_4 well is reported. If the septet surface is repulsive, then a picture such as that in Figure 4 is relevant. The stronger spin–orbit coupling in the 4d series, which lowers the adiabatic barrier relative to the diabatic surface crossing point, may explain why Mo reacts while Cr is inert.

The most recent *ab initio* calculations[4b] estimate barrier heights from ground-state M + C_2H_4 to the H–M–C_2H_3 bond insertion intermediate. They find a small barrier of 5 kcal/mol for Nb, a larger barrier of 15 kcal/mol for Y and Zr, and a very large barrier of 28 kcal/mol for Mo. Our experiments indicate that the absolute magnitudes of these barriers are too large, but the calculations are in good qualitative accord with the observed trend in reactivity from Y to Mo. The calculations suggest that the Y, Zr, and Mo reaction rates with C_2H_4 may be limited by the height of the barrier to C–H bond insertion. It will be interesting to learn the magnitude of calculated barrier heights to M(C_2H_4) complex formation; they may well follow the same trend.

Finally, we comment on the absence of M + *alkane* chemistry at 300 K for the entire 3d series and for all 4d series atoms studied thus far except Pd. Blomberg *et al.*[10] as well as Low and Goddard[11] have studied the activation of the C–H bond of methane and the C–C bond of ethane by several first- and second-row transition metal atoms. In particular, in the 4d series Blomberg obtains barriers to C–H insertion in the range 15–50 kcal mol^{-1}. This is consistent with the observed absence of M + alkane reactions at 300 K. For a given metal, the calculated barrier to C–C bond insertion is 15–20 kcal mol^{-1} larger than the barrier for C–H insertion. Activation barriers are considerably higher and binding energies are lower for 3d-series metals than for 4d-series metals due to weaker metal–carbon and metal–hydrogen bonds.[25] The $d^{x-1}s^1$ orbital occupancy dominates in the insertion product, just as it dominates the metallacyclopropane product from M + C_2H_4. While the electronic requirements for formation of metallacyclopropane from M + C_2H_4 and for formation of H–M–CH_3 from M + CH_4 are quite similar, the π bond broken in C_2H_4 is much weaker than the σ bond broken in CH_4. This may be why some neutral metal atoms can react with alkenes, but essentially none react with linear alkanes. The sole exception thus far is Pd, which apparently forms collisionally stabilized η^2 complexes with C_2H_6 and larger alkanes due to its unique $4d^{10}$ ground state.[7,8] Many of the 4d series atoms and Ni from the 3d series react with cyclopropane, presumably because of its weaker C–C bonds.

V. Conclusion

The nature of the interactions between bare, neutral transition metal atoms and alkanes and alkenes is becoming clearer. Probably none of the neutral metal atom ground states can insert in C–H or C–C bonds of linear alkanes at 300 K, although Y, Zr, Nb, and Pd react with cyclopropane. Reactions with alkenes are often facile, especially in the 4d series. For $4d^{x-2}5s^2$ ground states such as Y and Zr, the simple curve-crossing model of Figure 4 seems quite useful. The diabatic surface correlating with ground-state reactants is repulsive, and the promotion energy to metal atom excited states more suitable for chemical bonding is a major determinant of ground-state reactivity at 300 K. The $4d^45s$ ground state of Nb and the $4d^{10}$ ground state of Pd are unusually reactive with alkenes, apparently because deep M–alkene potential wells correlate with ground-state M + alkene for these atoms.

While the absence of pressure dependence of the M + alkene rate constants over the limited He range of 0.5–0.8 Torr strongly suggests that bimolecular, elimination chemistry is occurring, we have not yet identified the products. We will attempt to use one-photon ionization and time-of-flight mass spectrometry to measure the mass of the products. Further progress will continue to involve an interplay between theory and experiment.

Acknowledgment. We thank the National Science Foundation (CHE-9000503) and the donors of the Petroleum Research Fund, administered by the American Chemical Society, for generous support of this work.